Field-dependent ordered phases and Kondo phenomena in the filled skutterudite compound $PrOs_4As_{12}$

M. B. Maple[†‡§], N. P. Butch[†‡], N. A. Frederick[†‡], P.-C. Ho[‡], J. R. Jeffries[†‡], T. A. Sayles[†‡], T. Yanagisawa[‡], W. M. Yuhasz[‡¶], Songxue Chi[‖], H. J. Kang[††], J. W. Lynn[††], Pengcheng Dai[‖‡‡], S. K. McCall[§§], M. W. McElfresh[§§], M. J. Fluss[§§], Z. Henkie[¶¶], and A. Pietraszko[¶¶]

[†]Department of Physics, [‡]Institute for Pure and Applied Physical Sciences, and [¶]Materials Science and Engineering Program, University of California at San Diego, La Jolla, CA 92093; [‖]Department of Physics and Astronomy, University of Tennessee, Knoxville, TN 37996; [††]Center for Neutron Research, National Institute of Standards and Technology, Gaithersburg, MD 20899-8562; [‡‡]Condensed Matter Sciences Division, Oak Ridge National Laboratory, Oak Ridge, TN 37831; [§§]Lawrence Livermore National Laboratory, P.O. Box 808, Livermore, CA 94550; and [¶¶]Institute of Low Temperature and Structure Research, Polish Academy of Sciences, 50-950, Wrocław, Poland

This contribution is part of the special series of Inaugural Articles by members of the National Academy of Sciences elected on April 20, 2004.

Contributed by M. B. Maple, February 23, 2006

Electrical resistivity, specific heat, and magnetization measurements to temperatures as low as 80 mK and magnetic fields up to 16 T were made on the filled skutterudite compound $PrOs_4As_{12}$. The measurements reveal the presence of two ordered phases at temperatures below approximately 2.3 K and in fields below approximately 3 T. Neutron-scattering experiments in zero field establish an antiferromagnetic ground state <2.28 K. In the antiferromagnetically ordered state, the electronic-specific heat coefficient $\gamma \approx 1$ J/mol·K² below 1.6 K and $0 \leq H \leq 1.25$ T. The temperature and magnetic-field dependence of the electrical resistivity and specific heat in the paramagnetic state are consistent with single-ion Kondo behavior with a low Kondo temperature on the order of 1 K. The electronic-specific heat in the paramagnetic state can be described by the resonance-level model with a large zero-temperature electronic-specific heat coefficient that decreases with increasing magnetic field from approximately 1 J/mol·K² at 3 T to approximately 0.2 J/mol·K² at 16 T.

heavy fermion | Kondo effect | antiferromagnetism

The compound $PrOs_4As_{12}$ belongs to the family of filled skutterudites, which have the formula AT_4X_{12}, where A = alkali metal, alkaline earth, lanthanide, or actinide, T = Fe, Os, or Ir, and X = P, As, or Sb. Because the ions reside in an atomic cage with a large number of X nearest neighbors, the hybridization between the lanthanide filler ion localized 4f states and the conduction–electron states is appreciable, often resulting in strongly correlated electron phenomena. In a recent article (1), we reported a study of the physical properties of single crystals of the filled skutterudite compound $PrOs_4As_{12}$ between approximately 0.4 and 300 K by means of magnetization M, specific heat C, and electrical resistivity ρ measurements. The previous study revealed that the compound exhibits two (possibly three) ordered phases below approximately 2.5 K in zero field and approximately 3 T at zero temperature from kinks in M as a function of magnetic field H and temperature T. Features in the $\rho(T)$ and $C(T)$ data in zero field can be identified with transitions into the two ordered phases below 2.5 K. The magnetic susceptibility conforms to a Curie–Weiss law below approximately 20 K with an effective magnetic moment $\mu_{\text{eff}} = 2.77\ \mu_B$/formula unit consistent with a Γ_5 ground state in a cubic crystalline electric field and a cusp at approximately 2.5 K, indicative of antiferromagnetic (AFM) order. These results provide another example of the wide range of correlated electron ground states that are found in the Pr-based filled skutterudites, which include conventional (Bardeen, Cooper, Schrieffer) superconductivity (e.g., $PrRu_4Sb_{12}$) (2), unconventional superconductivity (e.g., $PrOs_4Sb_{12}$) (3, 4), heavy fermion behavior (e.g., $PrFe_4P_{12}$, $PrOs_4Sb_{12}$) (5–8), antiferroquadrupolar order (e.g., $PrFe_4P_{12}$, $PrOs_4Sb_{12}$), and magnetic order (e.g., $PrFe_4Sb_{12}$) (9, 10). In this article, we report measurements of the temperature dependence of the magnetization, specific heat, and electrical resistivity in magnetic fields as high as 16 T and neutron diffraction measurements in zero field on $PrOs_4As_{12}$.

Results

A magnetic neutron-scattering pattern was obtained by subtracting the intensity of the 4-K diffraction pattern from the 0.63-K pattern. Fig. 1*a* shows the outcome of this subtraction, with clear magnetic intensity at positions consistent with $(h + 0.5, k, l)$, where h, k, and l are the Miller indices of the cubic unit cell. The observed diffraction pattern suggests a magnetic unit cell doubled along one axis of the elementary structural cubic cell. Although the cubic crystal symmetry and the apparent anisotropy of the mixed single-crystal samples prevent a conclusive determination of the spin configuration by using the diffraction intensities, it is clear that the AFM lattice consists of (1,0,0) planes within which Pr ions couple ferromagnetically, while alternate planes have opposite magnetic moment orientations. The order parameter of the sample in the AFM phase was determined by measuring the T dependence of the magnetic intensity at $2\theta = 17.9^\circ$ in the range 0.5–3.4 K. Fig. 1*b* indicates a Néel temperature $T_N = 2.28$ K, in excellent agreement with magnetization measurements (1).

Specific heat divided by temperature C/T vs. T data for temperatures below 4 K and in magnetic fields up to 3 T are displayed in Fig. 2. Previous zero-field measurements revealed two low-T features in $C(T)$ (Fig. 2 *Inset*): a slight shoulder at $T_2 \approx 2.3$ K, on the high temperature side of a well defined peak at $T_1 \approx 2.2$ K (1). T_1 can be identified with the AFM transition observed in neutron scattering. As H is applied, the two anomalies observed in zero field gradually shift toward 0 K. The second anomaly decreases with field more quickly than the first and is not observed above 0.6 K by $H = 1.5$ T, whereas the first transition persists to nearly $H = 3$ T. Additionally, the magnitude of the second transition is lowered with increasing H, whereas the first evolves from a rounded shoulder at the lowest fields to a clear peak by $H = 0.75$ T, although the true character of the

Conflict of interest statement: No conflicts declared.

Abbreviations: AFM, antiferromagnetic; PM, paramagnetic; RLM, resonance level model; UCSD, University of California at San Diego; LLNL, Lawrence Livermore National Laboratory.

[§]To whom correspondence should be addressed. E-mail: mbmaple@physics.ucsd.edu.

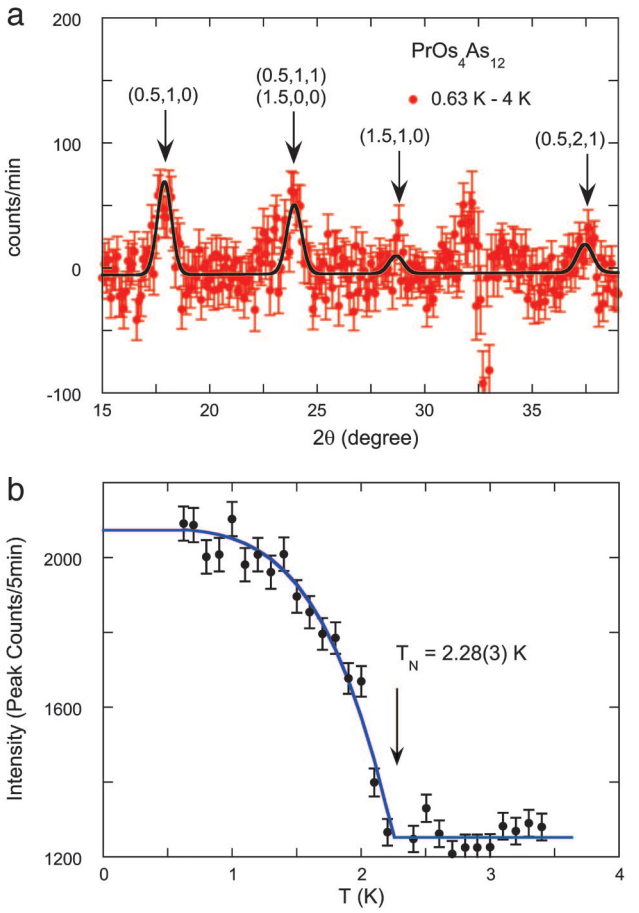

Fig. 1. Neutron diffraction measurements on $PrOs_4As_{12}$ at various temperatures between 0.63 and 4 K. (*a*) Intensity spectrum at 0.63 K after subtraction of the 4-K spectrum. The positive and negative intensities around $2\theta = 32^\circ$ represent imperfect subtraction around the nuclear Bragg peak (1,1,1) reflection. The positions of magnetic scattering are clearly marked, and the solid curve is a guide to the eye. (*b*) The T dependence of the (0.5,1,0) magnetic Bragg peak. The solid curve is a fit of mean field theory, yielding an estimated Néel temperature of 2.28 K.

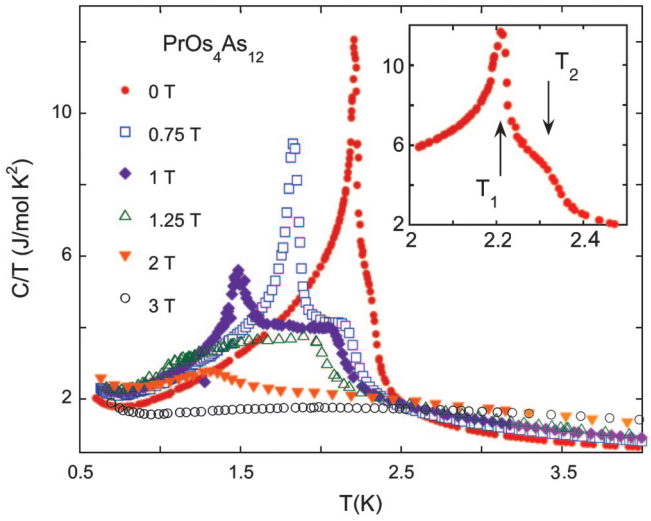

Fig. 2. Specific heat divided by temperature C/T vs. T in various magnetic fields H, showing the decrease of T_2 and T_1 with increasing H. (*Inset*) C/T vs. T in the zero field in the vicinity of the transition.

first anomaly at low H may be masked by the presence of the second. At the lowest temperatures, a slight upturn, associated with a nuclear Schottky anomaly, is visible. In fields strong enough to suppress the second transition, $H \geq 2$ T, a dome-like structure develops in $C(T)$ above the first transition (see Fig. 7), and the maximum of the dome decreases in magnitude and shifts to higher T with increasing H. These features are described in more detail in *Discussion*.

The features in $C(T)$ at low fields are also identified with features in $M(H, T)$ that have a similar field dependence, as described (1). Low-T $M(T)$ data for various values of H parallel to [111] are shown in Fig. 3. It has been reported that with increasing H, a peak in $M(T)$, denoted T_1, is suppressed toward $T = 0$ K, whereas a second peak in $M(T)$ at higher T, denoted T_2, splits off from T_1 and eventually shifts toward $T = 0$ K (1). Corresponding features were identified in $M(H)$ at constant T, as shown in Fig. 4 (1). Two kinks in $M(H)$, denoted H_1 and H_2, were found to be suppressed toward lower field with increasing T. The dc magnetic susceptibility $\chi_{dc}(T)$, reported in ref. 1 and shown in Fig. 4 *Inset*, displays a clear peak at $T = 2.3$ K, indicative of AFM ordering, consistent with the neutron-scattering measurement reported herein.

As reported in ref. 1, $\rho(T)$ was measured for 1.9 K $\leq T \leq$ 300 K in H up to 16 T (Fig. 5). It was shown that the zero-field $\rho(T)$ decreased with decreasing temperature, displayed a minimum at approximately 16 K, and then increased to a peak by approximately 5.5 K followed by a sharp decrease in the vicinity of the AFM transition (Fig. 5) (1). Measurements in an applied field (displayed in Fig. 5 *Inset a* and *Inset b*) reported herein reveal a negative magnetoresistance with increasing field below approximately 25 K. However, below 1.75 K, ρ increases with H, reaching a maximum at 1.5 T, then decreases with increasing H. Eventually the $\rho(H)$ curves at various constant T merge in the highest fields (Fig. 6). At $H = 1$ T, two features in the $d\rho/dT$ vs. T curves are associated with the two phase transitions at T_2 and T_1 (Fig. 6*a Inset*). Isotherms of $\rho(H)$, shown in Fig. 6*b*, display a peak that develops at $T < 2.3$ K, indicative of a field-induced transition at H_1. The peak shifts to higher fields with decreasing temperature, up to 1.5 T below 0.5 K. A change in slope, apparently caused by a field-induced transition to the paramagnetic (PM) state at H_2 (Fig. 6*b Inset*), was observed for $H > H_1$.

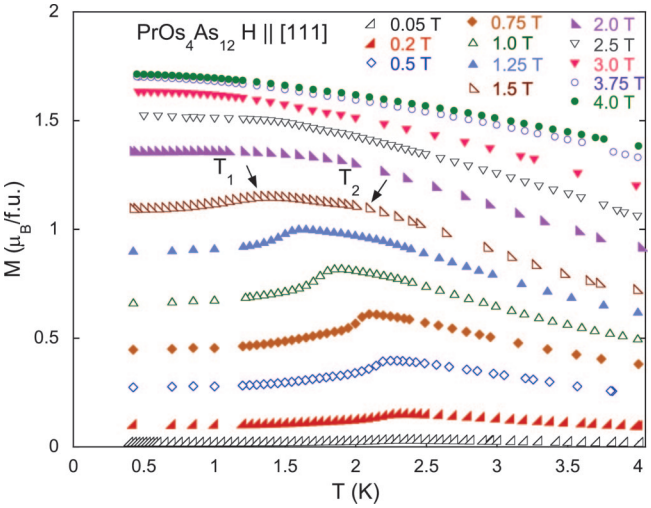

Fig. 3. Magnetization M vs. T for several values of H. Features in $M(T)$ at constant H, with T_2 defined by a small peak, and T_1 defined by the prominent peak, are illustrated for $H = 1.5$ T.

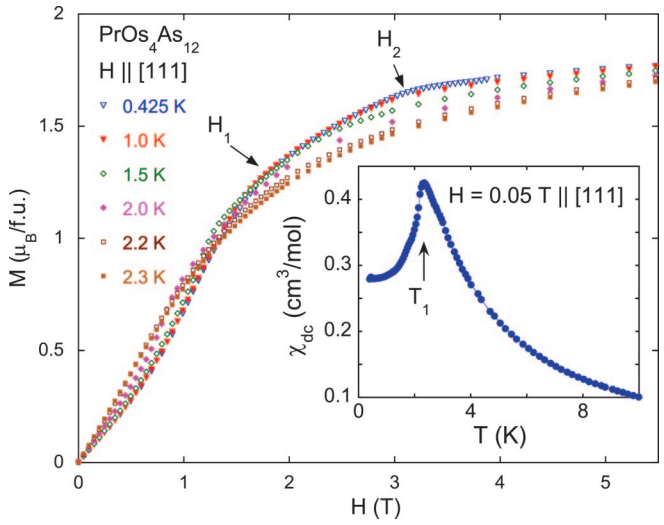

Fig. 4. Magnetization M vs. H isotherms for several values of T. Features in $M(H)$ at constant T, with H_1 and H_2 defined by a kink in the slope, are illustrated for $PrOs_4As_{12}$, which indicates a magnetic transition at 2.3 K. (*Inset*) DC magnetic susceptibility χ_{dc} vs. T for $PrOs_4As_{12}$.

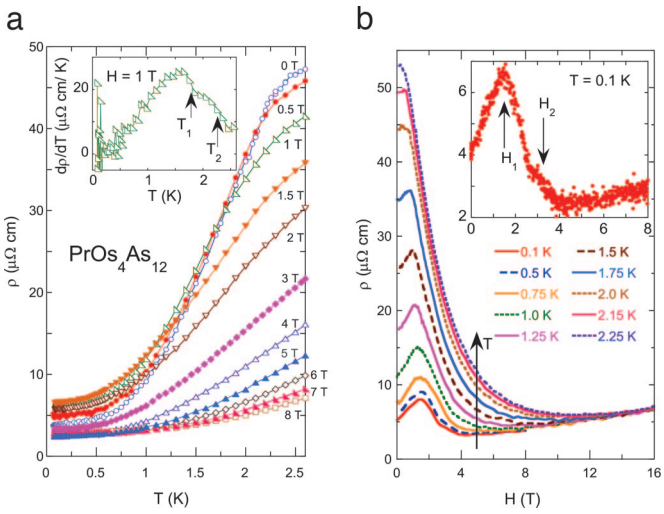

Fig. 6. Electrical resistivity ρ measurements as a function of temperature T and magnetic field H for $PrOs_4Ps_{12}$. (*a*) Low-temperature electrical resistivity ρ vs. T for $0\ T \leq H \leq 8$ T. (*Inset*) T_2 and T_1 as determined from features in $d\rho/dT$ vs. T at 1 T. (*b*) Isotherms of ρ vs. H. (*Inset*) An expanded view of the 0.1-K $\rho(H)$ isotherm with two linear fits indicating a break in slope at 2.56 T.

Discussion

Contributions to Specific Heat. In ref. 1, the specific heat was analyzed in zero field. The low-T zero-field-specific heat was assumed to consist of four terms, $C(T) = C_n(T) + C_e(T) + C_l(T) + C_m(T)$, which are the nuclear Schottky, electronic, lattice, and magnetic contributions, respectively. At higher temperatures, where $C_m(T)$ and $C_n(T) \approx 0$, the specific heat was dominated by the electronic and lattice terms. A fit of $C/T = \gamma + \beta T^2$ to the data in the range $10\ K \leq T \leq 18$ K yielded an enhanced electronic specific heat coefficient $\gamma = 211$ mJ/mol·K^2 and, from β, a Debye temperature $\theta_D = 260$ K (1). The calculated magnetic entropy $S_m(T)$ leveled off to a value of 90% $Rln3$ by 8 K (1).

Analysis of the zero-field specific heat ΔC, after subtraction of the lattice contribution, was based on an expression of the following form, $\Delta C(T) = C_n(T) + C_e(T) + C_m(T)$ (1), where $C_n(T) = A/T^2$, $C_e(T) = \gamma T$, and $C_m(T) = BT^n$. In zero field, it was found that $A = 128$ mJ·K/mol, $n = 3.2 \pm 0.1$, and $\gamma \approx 1$ J/mol·K^2 (1). As stated in ref. 1, the discrepancy between the value of γ estimated from these fits to $\Delta C(T)$ in the ordered phase and the γ value taken from the earlier fit to $C(T)$ in the PM state is likely caused by a T dependence of the electronic contribution to the specific heat, as has been observed in a number of heavy fermion systems (11). Fits of this form have now been performed in the ordered state ($T < 0.6\ T_1$) in field. Analysis of $\Delta C(T)$ in an applied field reveals that A increases monotonically to $A = 215$ mJ·K/mol by 1.25 T, n does not change substantially with field, and γ remains close to 1 J/mol·K^2.

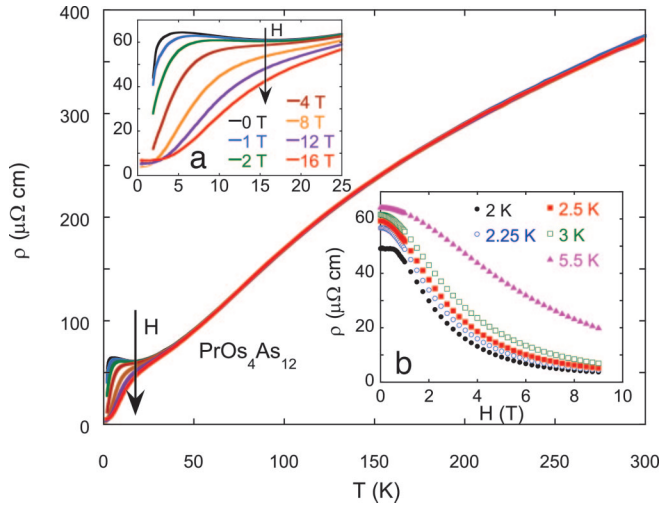

Fig. 5. Electrical resistivity ρ vs. T from 2 to 300 K at various fields H. (*Inset a*) $\rho(T)$ from 2 to 25 K. (*Inset b*) $\rho(H)$ at various temperatures around T_2.

Single-Ion Kondo Behavior. For $H \geq 3$ T, a broad maximum was observed in $C_e(T)$, reminiscent of that observed in $C_e(T)$ for $PrFe_4P_{12}$ (6). Therefore, the $C_e(T)$ data for $PrOs_4As_{12}$ were analyzed in terms of the resonance-level model (RLM) of Schotte and Schotte (12) used in ref. 6 for $PrFe_4P_{12}$. This model has three parameters: the width of a Lorentzian peak in the density of states $\Delta \approx k_B T_K$ (where T_K is the Kondo temperature), the spin S, and a Zeeman term gH associated with the applied field, although it was also necessary to scale the curves by a factor f. The parameters S, Δ, and f were held fixed for all fields, while the term gH was varied. Three spin values, $S = 1/2$, 1, and 3/2, give reasonable fits; however, $S = 1$ results in the best fits and was consistent with the entropy released, as well as the proposed crystalline electric field split Pr^{3+} Γ_5 triplet ground state (1). The best results are found for $T_K \approx 3.5$ K and $f \approx 1.3$ for the University of California at San Diego (UCSD) data and $T_K \approx 5$ K and $f \approx 1.6$ for the Lawrence Livermore National Laboratory (LLNL) data. Fig. 7 shows the high field data and the corresponding fits to the RLM with $S = 1$. In zero field, the Zeeman parameter $gH = 0$ and it monotonically increases with H, as expected, because the fits were applied only to data in the PM state. However, gH is a linear function of H only below 5 T, with $g = 3.4$, whereas in $H > 5$ T, g decreases to a value of ≈1.7. This nonlinearity may be caused by the inaccuracy of the single-ion description of what is actually a cooperative phenomenon in $PrOs_4As_{12}$. That the RLM roughly describes the $C(T)$ data likely reflects generic behavior associated with a sharply peaked electronic density of states at the Fermi level, whereas a Lorentzian distribution is a coarse approximation of the actual density of

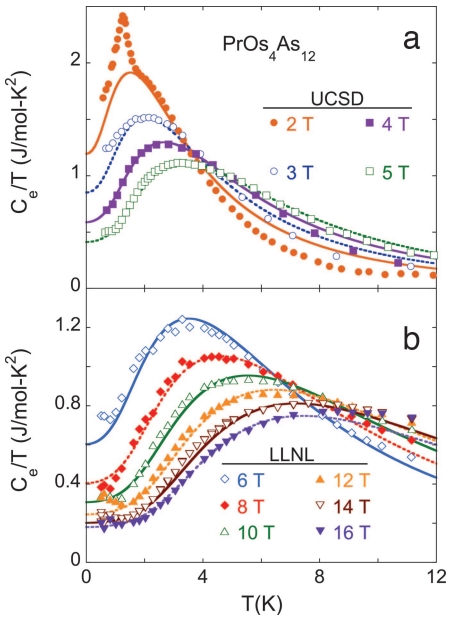

Fig. 7. The electronic contribution to the specific heat divided by temperature, C_e/T, vs. T for 2 T $\leq H \leq$ 5 T (*a*) and 6 T $\leq H \leq$ 16 T (*b*). The data at $H \leq$ 5 T were taken at UCSD, whereas the data at $H \geq$ 6 T were taken at LLNL. Fits to the RLM are presented, as described in *Discussion*.

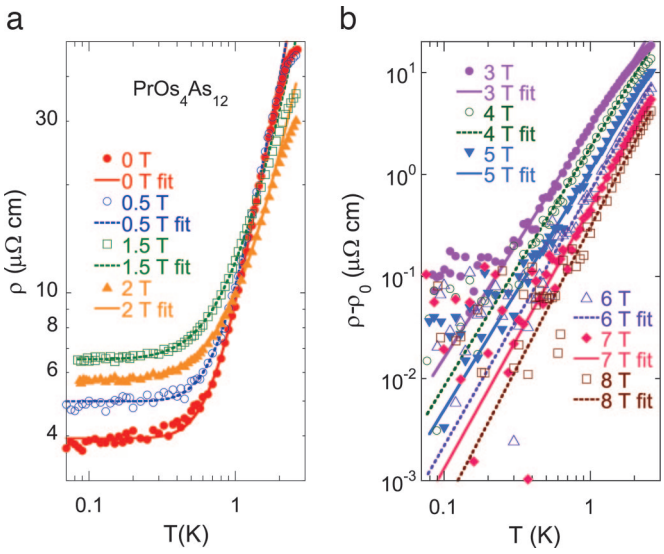

Fig. 9. Analysis of the low-temperature electrical resistivity P (T) of $PrOs_4As_{12}$ in terms of an antiferromagnet with an energy gap (*a*) and a power law in T (*b*). (*a*) Low-temperature electrical resistivity ρ vs. T for $H \leq$ 2 T fit by a function describing the resistivity of an AFM metal with an energy gap. (*b*) Plot of $\log(\rho - \rho_0)$ vs. $\log T$, where ρ_0 is the residual resistivity, with linear fits corresponding to power-law T dependencies.

states in $PrOs_4As_{12}$ that renders the RLM inaccurate even at moderate H. For this reason, the values of g estimated from the RLM fits cannot be regarded as accurate.

Despite the aforementioned caveats, the RLM was used to estimate the value that $\gamma(0)$ would have if $PrOs_4As_{12}$ were to remain in the PM phase at $T = 0$ K in $H < 3$ T rather than undergoing transitions into ordered phases. In this analysis, the parameters S, Δ, and f were assumed to have the same values as they have in $H > 3$ T. The RLM fits describe the $C_e(T)$ data in the PM phase, but obviously deviate from the $C_e(T)$ data in the ordered phases. The resulting C_{RLM}/T values at $T \approx 0$ for all fields are plotted in Fig. 8 along with γ values estimated from the

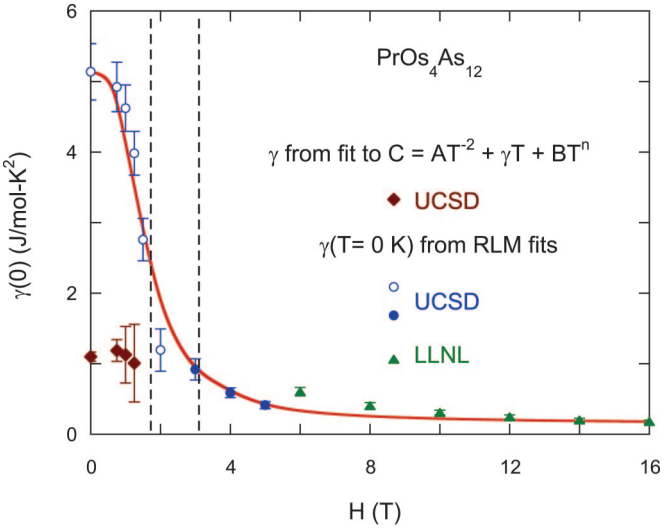

Fig. 8. The $T = 0$ K value of the coefficient of the electronic part of the specific heat $\gamma(0)$ vs. H; the circles and triangles represent the $T = 0$ K value of RLM fits to the data taken at UCSD and LLNL, respectively. The solid line is a guide to the eye, and the dashed lines represent the critical fields H_1 and H_2. Diamonds represent values of γ estimated from $\Delta C(T)$ in the ordered state.

fits to $\Delta C(T)$ data in the ordered state. In Fig. 8 the open circles represent values of $\gamma(0)$ derived from fits of the RLM to the $C_e(T)$ data only in the PM phase, $T > T_2$ in $H < 3$ T. As calculated by the RLM fits, $\gamma(0)$ peaks in zero field and decreases sharply with increasing H, leveling off once the PM state is entered. In contrast, the fits to $\Delta C(T)$ in the ordered state yield values of $\gamma \approx 1$ J/mol·K^2 (1), similar in magnitude to $\gamma(0)$ values from the RLM fits to the 2-T and 3-T $C_e(T)$ data. These results suggest that upon entering the AFM phase at low T the triply degenerate Kondo-like resonance splits because of the development of an effective internal field, which reduces the electronic density of states at the Fermi level, thus decreasing the electronic contribution to $C(T)$. Because the RLM predicts $\gamma(T = H = 0) = 5$ J/mol·K^2, it may be argued that the AFM ground state "shields" the system from the massive itinerant electronic degeneracy that would exist at low T in the absence of resonance splitting. It should be noted that attempts were made to fit the broad feature in $C_e(T)$ with Schottky anomalies caused by crystalline electric field split Pr^{3+} states, but those fits were unable to reproduce the feature.

At the lowest temperatures, $\rho(T)$ in $PrOs_4As_{12}$ is not dominated by electron–electron scattering (ρ goes as T^2) or simple AFM magnon scattering (ρ goes as T^5), but is described well by an expression for an antiferromagnet with an energy gap Δ in the magnon spectrum (13):

$$\rho(T) = \rho_0 + b\left(\frac{T}{\Delta}\right)\left(1 + 2\frac{T}{\Delta}\right)e^{-\Delta/T}. \quad [1]$$

The $\rho(T)$ data are fit well by Eq. **1** for $H < 2$ T (Fig. 9*a*), and a plot of the energy gap Δ vs. H is shown in Fig. 10*a*. Notably, the value of Δ drops sharply near 1.5 T in the vicinity of the transition at H_1. To check for possible non-Fermi-liquid behavior associated with a field-tuned phase transition ($H \geq 3$ T), the $\rho(T)$ data in $H \leq 8$ T were also fit with a power-law $\rho(T) = \rho_0 + BT^n$ (Fig. 9*b*). The residual resistivity ρ_0 has a pronounced maximum at $H = 1.5$ T, corresponding to H_1 (Fig. 10*c*). The power-law exponent n decreases from approximately 2.9 to approximately 2.3 as H increases from 0 to 2 T, reaches a minimum between 2

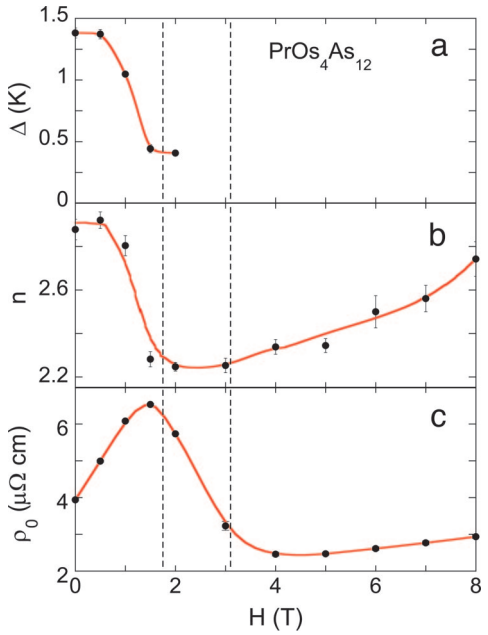

Fig. 10. Parameters from the analyses of the 10W-temperature electrical resistivity data shown in Fig. 9. (*a*) Energy gap Δ from the fits of Eq. **1** (Fig. 9*a*). (*b*) Residual resistivity ρ_0 vs. *H*. (*c*) Exponent *n* of power-law fit vs. *H* (Fig. 9*b*). The solid lines are guides to the eye, and the dashed lines represent the critical fields H_1 and H_2.

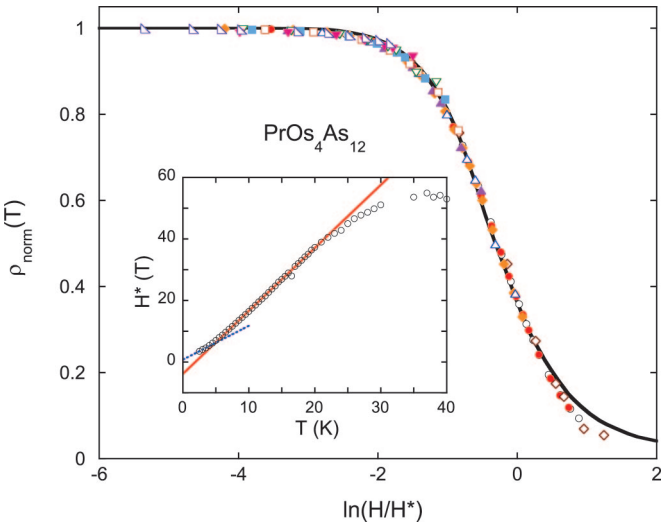

Fig. 11. Normalized electrical resistivity ρ_{norm} (defined in text) vs. ln[$H(T)$/$H^*(T)$] for $PrOs_4As_{12}$. The solid line represents Schlottmann's $J = 1$ scaling curve (18), and the various symbols represent $\rho(H)$ isotherms ranging from 2.5 to 40 K. (*Inset*) Characteristic Kondo field H^* vs. *T*. The solid line represents a high-*T* linear fit with $H^* = -3.86$ [T] + 2.05 [T/K] T, and the dashed line represents a low-temperature fit with $H^* = 0.78$ [T] + 1.1 [T/K] T.

and 3 T, then gradually increases to ≈2.8 when *H* reaches 8 T (Fig. 10*b*). In no range of *H* does $PrOs_4As_{12}$ display the $T^{3/2}$ non-Fermi-liquid behavior predicted to occur near a 3D AFM quantum critical point (14).

For $H < 4$ T in the PM state, the $\rho(T)$ data exhibit a local minimum at approximately 16 K (Fig. 5), while the $\rho(H)$ curves decrease with increasing *H* and $\rho(H = 0) - \rho(H)$ decreases rapidly as *T* increases; this behavior is consistent with the Kondo effect (15–17). To determine whether $PrOs_4As_{12}$, which shows Kondo lattice behavior, can be described in the PM regime by the single-ion Kondo impurity model, a scaling analysis developed by Schlottmann (18) was applied to the $\rho(H, T)$ data. A lattice contribution $\rho_l(T)$ [estimated from $LaOs_4Sb_{12}$ (24)] was subtracted before the data were scaled, although it was subsequently found that it makes little difference whether this correction is made. Fig. 11 displays the dependence of the normalized magnetoresistivity $\rho_{norm}(T) = [\rho(H, T) - \rho_l(T)]/[\rho(H = 0, T) - \rho_l(T)]$ on the scaled magnetic field $H/H^*(T)$ in the PM state, where $H^*(T)$ is the characteristic *T*-dependent Kondo field. The scaling of the magnetoresistivity of $PrOs_4As_{12}$ agrees well with Schlottmann's $J = 1$ scaling curve (18), in accordance with a Γ_5 triplet ground state inferred from magnetization and specific heat data. The values of H^* deduced from the scaling analysis are plotted vs. *T* in Fig. 11 *Inset*; H^* is approximately linear in the temperature regime from 6 to 22 K, whereas below 6 K and above 22 K, $H^*(T)$ has shallower slopes.

In the single impurity model, $H^*(T)$ is given by the relation

$$H^*(T) = H^*(0) + \frac{k_B T}{g_J \mu_{ion}} = \frac{k_B}{g_J \mu_{ion}} (T_K + T), \qquad [2]$$

where $H^*(0)$ is the zero-*T* characteristic Kondo field, T_K is the Kondo temperature, g_J is the Landé *g* factor ($g_J = 0.8$ for the Pr^{3+} ion), and μ_{ion} is the ionic local magnetic moment (16, 17). A linear fit between 6 and 22 K resulted in a $\mu_{ion} = 0.91\mu_B$ and $H^*(0) = -3.86$ T, corresponding to $T_K = -1.88$ K, although typically one would expect a positive value for $H^*(0)$ and T_K. Possible explanations for this discrepancy are: (*i*) The single-ion model is too simplified for this Kondo-lattice system. Similar results were obtained previously in the case of UBe_{13} (15). (*ii*) The Kondo temperature is not constant <40 K, which is evident in the curvature of $H^*(T)$. (*iii*) If the lowest three values of H^* at 2.5, 3, and 3.5 K are used to estimate T_K, a positive $T_K \approx 0.7$ K is obtained [$\mu_{ion} = 1.68\ \mu_B$ and $H^*(0) = 0.77$ T]. (*iv*) Magnetic correlations persist into the PM state. In any case, this scaling analysis indicates that the Kondo temperature is small, and that the Kondo effect in $PrOs_4As_{12}$ is sensitive to magnetic correlations.

Phase Diagram. The features in $C(H,T)$ (Fig. 2), $M(H, T)$ (Figs. 3 and 4), and $\rho(H, T)$ (Fig. 6) associated with T_2, T_1, H_1, and H_2 have been used to generate an *H*–*T* phase diagram for $PrOs_4As_{12}$ (Fig. 12). The bars in Fig. 12 are rough estimates of the transition widths, based on the widths of those features. Comparing the magnetic, resistive, and thermodynamic phase diagrams, it is likely that the higher-field *M* features, which correspond to peaks in $M(T)$ (T_2 and T_1) and kinks in $M(H)$ (H_1 and H_2) are associated with the peaks in $C(T)$ (T_2 and T_1) and features in $\rho(H)$ (H_1 and H_2). Although the values of *H* at which the phase boundaries are defined for different measurements differ by as much as 0.5 T, the field dependence of the features is very similar. These discrepancies are caused partly by measurement-dependent differences in the definitions of the various transitions and variations between samples, in addition to the fact that $M(H,T)$ and $C(H,T)$ measurements were performed on a collection of crystals.

Nonetheless, it may be inferred from the strong peaks in $C(T)$ that there are two bulk-phase transitions: $PrOs_4As_{12}$ has an AFM ground state, a different ordered state OP2 at intermediate *T* and *H*, and a PM state at high *T* and *H*. Previously, features in $M(H, T)$ and crystalline electric field considerations were argued to support an AFM ground state (1). Neutron scattering has now confirmed AFM order in this phase. Analysis of $\rho(H, T)$ data shows evidence for an energy gap that closes at H_1, whereas ρ_0 goes through a maximum at H_1 (Fig. 10), which is consistent with enhanced scattering off

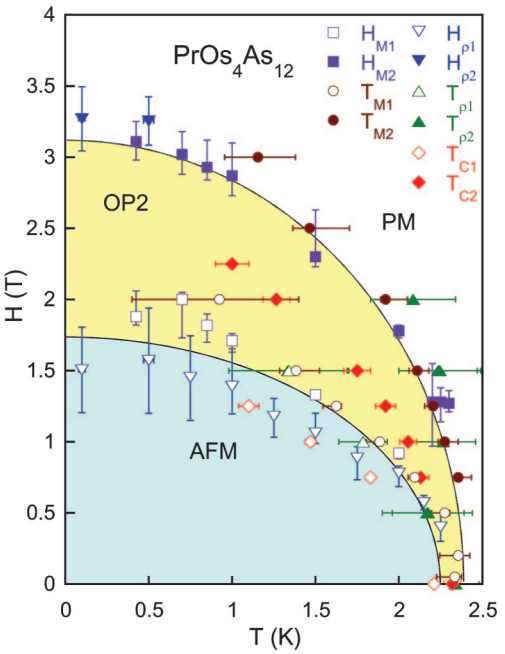

Fig. 12. Magnetic field-temperature (*H-T*) phase diagram for $PrOs_4As_{12}$, as defined by features in magnetization *M* (Figs. 3 and 4) (circles and squares), specific heat *C* (Fig. 2) (diamonds), and electrical resistivity ρ (Fig. 6) (triangles). The lines are guides to the eye, separating the PM region from the ordered phases (AFM and OP2).

of critical fluctuations at a magnetic phase transition. A triplet ground state is supported by compelling evidence from $M(H, T)$ data and the Kondo-resonance-based analysis of $C(H, T)$ and $\rho(H, T)$. The recent measurements in magnetic field were unable to determine the ordering that occurs in OP2; however, as stated in ref. 1, quadrupolar or magnetic ordering remain likely candidates for OP2.

Comparison to $PrFe_4P_{12}$. Numerous compounds exhibit features similar to those observed in $PrOs_4As_{12}$. The most noteworthy example is $PrFe_4P_{12}$, which, like $PrOs_4As_{12}$, is a Pr-based filled skutterudite compound that displays heavy fermion behavior and AFM-like features (19, 20). The electrical resistivities of these two compounds display a Kondo-like minimum and a sharp downturn below their respective ordering temperatures. A negative magnetoresistance is also observed in these compounds in the vicinity of their respective ordering temperatures (21). At 5 T, the magnitude of the magnetization of both $PrFe_4P_{12}$ and $PrOs_4As_{12}$ below their transition temperatures is much less than the Pr^{3+} free-ion value of 3.2 μ_B/Pr ion; however, there is a clear step-like feature in the $M(H)$ data for $PrFe_4P_{12}$, indicating a metamagnetic transition (19), whereas features in the $M(H)$ data for $PrOs_4As_{12}$ are much more subtle. In high fields, the $C(T)/T$ data for both systems display a broad dome-shaped anomaly at low temperatures, but in zero field there is no indication of a second-phase transition in the $C(T)/T$ data for $PrFe_4P_{12}$ (6). Because neutron diffraction measurements of $PrFe_4P_{12}$ in zero field did not find any indication of long-range magnetic order and measurements in an applied field have revealed the presence of an induced AFM moment, antiferroquadrupolar ordering is speculated as being the source of the observed behavior of $PrFe_4P_{12}$ below 6.5 K (7, 22). The transition in $PrFe_4P_{12}$ at 6.5 K is also accompanied by a structural change that occurs at the same temperature (23).

Summary

Neutron diffraction measurements of $PrOs_4As_{12}$ in zero field confirm that the ground state is AFM, with $T_N = 2.28$ K. Features in the $C(H, T)$ and $\rho(H, T)$ data can be identified with transitions between two ordered phases and yield an *H–T* phase diagram similar to that inferred from the $M(H, T)$ data previously reported (1). The *T* dependence of ρ in the AFM ground state is consistent with the scattering of electrons by magnons with a gapped spectrum. Features reminiscent of single-ion Kondo behavior are observed in the PM state. The specific heat can be described in terms of the RLM for spin $S = 1$, which would be appropriate for a Pr^{3+} triplet ground state, yielding a Kondo temperature of approximately 3 K. Moreover, $\rho(H, T)$ scales with H/H^* and is consistent with a small $T_K < 1$ K and a triplet ground state.

Experimental Details

Single crystals of $PrOs_4As_{12}$ were grown by means of a molten metal flux method at high temperatures and pressures as described (1). Neutron diffraction measurements were performed on the triple-axis spectrometer BT2 at the National Institute of Standards and Technology Center for Neutron Research. The small single-crystal samples (approximately 1 mm in size) with a total mass of approximately 1.2 g were wrapped in thin aluminum foil and sealed inside a thin-wall aluminum can mounted in a ^{3}He cryostat.

The incident and final neutron energies were set to 14.7 meV with pyrolytic graphite as monochromator, analyzer, and filters. The collimations were 60 minutes of arc-40 minutes of arc-sample -40 minutes of arc-open from the reactor to the detector. Scans were carried out at 0.63 and 4 K with the angle 2θ ranging from 3° to 65° with a step size of 0.1°.

Specific heat $C(T)$ measurements on $PrOs_4As_{12}$ were performed for 0.5 K $\leq T \leq$ 18 K in *H* up to 5 T at UCSD in a semiadiabatic ^{3}He calorimeter. Initial measurements in zero field were performed on a collection of single crystals with a total mass of 49 mg, while additional measurements in zero and higher fields were performed on a collection of single crystals with a mass of 29 mg. The calculated molar specific heats of the two zero-field measurements were found to be identical within experimental error. Additional $C(T)$ measurements for 0.4 K $\leq T \leq$ 20 K in *H* up to 16 *T* were performed at LLNL in a Quantum Design (San Diego) ^{3}He Physical Property Measurement System (PPMS). Bulk magnetization *M* for temperatures 0.4 K $\leq T \leq$ 10 K and applied magnetic fields -5.5 T $\leq H \leq$ 5.5 T was measured in a ^{3}He Faraday magnetometer. A mosaic of 27 crystals, with a total mass of 27 mg, was measured with the [111] axis of the crystals nominally aligned parallel to *H*. Measurements of $M(T, H)$ were also performed by using a Quantum Design Magnetic Property Measurement System in *H* up to 5.5 T for 1.7 K $\leq T \leq$ 300 K. Electrical resistivity $\rho(H, T)$ measurements were made by using a four-probe ac technique in fields up to 9 T for 2 K $\leq T \leq$ 300 K in a Quantum Design PPMS by using a constant current of 1–10 mA and in *H* up to 8 T for 0.06 K $\leq T \leq$ 2.6 K by using a ^{3}He-^{4}He dilution refrigerator and a constant current of 300 μA, with *H* perpendicular to the electrical current and parallel to the [100] axis. Additional $\rho(H, T)$ measurements for 0.5 K $\leq T \leq$ 300 K in *H* up to 16 T were performed at LLNL in a Quantum Design ^{3}He PPMS by using a constant current of 0.25–1 mA.

Research at UCSD was supported by Department of Energy Grant DE-FG02-04ER46105 and National Science Foundation Grant DMR 0335173. Work at the National Institute of Standards and Technology was supported by Department of Energy Grants DE-FG02-05ER46202 and DE-AC05-00OR22725 at the University of Tennessee/Oak Ridge National Laboratory. Work at LLNL was performed under Department of Energy Contract W-7405-Eng-48. T.Y. was supported by a Japan Society for the Promotion of Science Postdoctoral Fellowship for Research Abroad.

1. Yuhasz, W. M., Butch, N. P., Sayles, T. A., Ho, P.-C., Jeffries, J. R., Yanagisawa, T., Frederick, N. A., Maple, M. B., Henkie, Z., Pietraszko, A., *et al.* (2006) *Phys. Rev. B*, in press.
2. Takeda, N. & Ishikawa, M. (2000) *J. Phys. Soc. Jpn.* **69,** 868–873.
3. Bauer, E. D., Frederick, N. A., Ho, P.-C., Zapf, V. S. & Maple, M. B. (2002) *Phys. Rev. B* **65**, 100506-1–100506-4.
4. Maple, M. B., Ho, P.-C., Zapf, V. S., Frederick, N. A., Bauer, E. D., Yuhasz, W. M., Woodward, F. M. & Lynn, J. W. (2002) *J. Phys. Soc. Jpn.* **71,** Suppl., 23–28.
5. Curnoe, S. H., Harima, H., Takegahara, K. & Ueda, K. (2002) *Physica B* **312–313,** 837–839.
6. Aoki, Y., Namiki, T., Matsuda, T. D., Abe, K., Sugawara, H. & Sato, H. (2002) *Phys. Rev. B* **65**, 064446-1–064446-7.
7. Hao, L., Iwasa, K., Nakajima, M., Kawana, D., Kuwahara, K., Kohgi, M., Sugawara, H., Matsuda, T. D., Aoki, Y. & Sato, H. (2003) *Acta Phys. Pol. B* **34,** 1113–1116.
8. Tayama, T., Custers, J., Sato, H., Sakakibara, T., Sugawara, H. & Sato, H. (2004) *J. Phys. Soc. Jpn.* **73,** 3258–3261.
9. Bauer, E., Berger, S., Paul, C., Della Mea, M., Hilscher, G., Michor, H., Reissner, M., Steiner, W., Grytsiv, A., Rogl, P. & Scheidt, E. W. (2002) *Phys. Rev. B* **66,** 214421-1–214421-9.
10. Butch, N. P., Yuhasz, W. M., Ho, P.-C., Jeffries, J. R., Frederick, N. A., Sayles, T. A., Zheng, X. G., Maple, M. B., Betts, J. B., Lacerda, A. H., *et al.* (2005) *Phys. Rev. B* **71,** 214417-1–214417-11.
11. Maple, M. B., Bauer, E. D., Zapf, V. S. & Wosnitza, J. (2004) in *Superconductivity in Nanostructures, High T_C and Novel Superconductors, Organic Superconductors*, eds. Bennemann, K. H. & Ketterson, J. B. (Springer, Berlin), Vol. II, pp. 555–730.
12. Schotte, K. D. & Schotte, U. (1975) *Phys. Lett.* **55,** 38–40.
13. Andersen, N. H. (1980) in *Crystalline Electric Field and Structural Effects in F-Electron Systems*, eds. Crow, J. E., Guertin, R. P. & Mihalisin, T. W. (Plenum, New York), pp. 373–387.
14. Millis, A. J. (1993) *Phys. Rev. B* **48,** 7183–7196.
15. Batlogg, B., Bishop, D. J., Bucher, E., Golding, B., Jr., Ramirez, A. P., Fisk, Z., Smith, J. L. & Ott, H. R. (1987) *J. Magn. Magn. Mater.* **63–64,** 441–446.
16. Bauer, E., Gratz, E., Maikis, M., Kirchmayr, H., Roy, S. B. & Coles, B. R. (1993) *Physica B* **186–188,** 586–589.
17. Yamauchi, R. & Fukamichi, K. (2000) *J. Phys. Condens. Matter* **12,** 2461–2468.
18. Schlottmann, P. (1983) *Z. Phys. B Condens. Matter* **51,** 223–235.
19. Torikachvili, M. S., Chen, J. W., Dalichaouch, Y., Guertin, R. P., McElfresh, M. W., Rossel, C., Maple, M. B. & Meisner, G. P. (1987) *Phys. Rev. B* **36,** 8660–8664.
20. Sugawara, H., Matsuda, T. D., Abe, K., Aoki, Y., Sato, H., Nojiri, S., Inada, Y., Settai, R. & Ōnuki, Y. (2001) *J. Magn. Magn. Mater.* **226–230,** 48–50.
21. Kuramochi, E., Sugawara, H., Matsuda, T. D., Abe, Y., Abe, K., Aoki, Y. & Sato, H. (2003) *Acta Phys. Pol. B* **34,** 1129–1132.
22. Keller, L., Fischer, P., Herrmannsdörfer, T., Dönni, A., Sugawara, H., Matsuda, T. D., Abe, K., Aoki, Y. & Sato, H. (2001) *J. Alloys Compound* **323–324,** 516–519.
23. Lee, C. H., Matsuhata, H., Yamamoto, A., Ohta, T., Takazawa, H., Ueno, K., Sekine, C., Shirotani, I. & Hirayama, T. (2001) *J. Phys. Condens. Matter* **13,** L45–L48.
24. Shirotani, I., Ohno, K., Sekine, C., Yagi, T., Kawakami, T., Nakanishi, T., Takahashi, H., Tang, J., Matsushita, A. & Matsumoto, T. (2000) *Phys B* **281–282,** 1021–1023.